Experimental and Theoretical Study of Deprotonation of DNA Adenine Cation Radical

Jia-long Jie, Chen Wang, Hong-mei Zhao, Di Song, and Hong-mei Su

Citation: Chinese Journal of Chemical Physics **30**, 664 (2017); doi: 10.1063/1674-0068/30/cjcp1710198
View online: https://doi.org/10.1063/1674-0068/30/cjcp1710198
View Table of Contents: http://cps.scitation.org/toc/cjp/30/6
Published by the American Institute of Physics

ARTICLE

Experimental and Theoretical Study of Deprotonation of DNA Adenine Cation Radical†

Jia-long Jie[a,c], Chen Wang[b], Hong-mei Zhao[a], Di Song[a*], Hong-mei Su[a,b*]

a. Institute of Chemistry, Chinese Academy of Sciences, Beijing 100190, China
b. College of Chemistry, Beijing Normal University, Beijing 100875, China
c. University of Chinese Academy of Sciences, Beijing 100049, China

(Dated: Received on October 11, 2017; Accepted on November 16, 2017)

Among all the DNA components, extremely redox-active guanine (G) and adenine (A) bases are subject to facile loss of an electron and form cation radicals ($G^{+\cdot}$ and $A^{+\cdot}$) when exposed to irradiation or radical oxidants. The subsequent deprotonation of $G^{+\cdot}$ and $A^{+\cdot}$ can invoke DNA damage or interrupt hole transfer in DNA. However, compared with intensive reports for $G^{+\cdot}$, studies on the deprotonation of $A^{+\cdot}$ are still limited at present. Herein, we investigate the deprotonation behavior of $A^{+\cdot}$ by time-resolved laser flash photolysis. The deprotonation product of $A(N_6\text{-}H)^{\cdot}$ is observed and the deprotonation rate constant, $(2.0\pm0.1)\times10^7$ s^{-1}, is obtained at room temperature. Further, the deprotonation rate constants of $A^{+\cdot}$ are measured at temperatures varying from 280 K to 300 K, from which the activation energy for the N_6-H deprotonation is determined to be (17.1±1.0) kJ/mol by Arrhenius equation. In addition, by incorporating the aqueous solvent effect, we perform density functional theory calculations for $A^{+\cdot}$ deprotonation in free base and in duplex DNA. Together with experimental results, the deprotonation mechanisms of $A^{+\cdot}$ in free base and in duplex DNA are revealed, which are of fundamental importance for understanding the oxidative DNA damage and designing DNA-based electrochemical devices.

Key words: DNA adenine, Deprotonation rate constant, Activation energy barrier, Density functional theory calculation

I. INTRODUCTION

Deoxyribonucleic acid (DNA) is an important substance that carries the genetic instructions used in the growth, development, functioning and reproduction of all known living organisms. Photoexcitation or potent radical oxidants can induce the DNA damage events [1−5] that are associated with degenerative diseases, cancer, and aging [6, 7]. Among all the components (nucleobase, deoxyribose, and phosphate) of DNA, the base is the most vulnerable to oxidative damage. Generally speaking, the electron-loss center in DNA base will generate a hole, resulting in the base cation radical [1, 2, 8−13]. Extensive studies have shown that the base cation radical is more acidic than its natural structure, and easily deprotonates to form the base neutral radical [1, 2, 4, 8−13]. The deprotonation will lead to a variety of DNA lesion products, affecting structures and functions of DNA molecules and potential applications in electrochemical devices [13, 14]. In this context, knowing the deprotonation mechanism of the base cation radical is critically important to understand relevant processes in DNA oxidative damage and DNA-based molecular electronics devices.

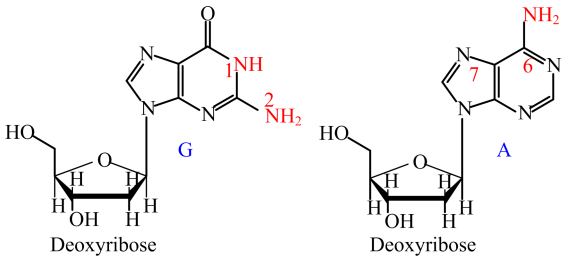

FIG. 1 The molecular structures of Guanine (G) and Adenine (A).

With the lowest oxidation potential among the four bases, Guanine (G) ($E^{\ominus}$=1.29 V *vs.* NHE) is extremely redox-active [1, 2, 8, 9, 15]. The oxidation to $G^{+\cdot}$ and the subsequent deprotonation process of $G^{+\cdot}$ have been the subjects of considerable experimental and theoretical studies [1, 2, 4, 8−10, 13, 14, 16, 17]. As shown in FIG. 1, $G^{+\cdot}$ has two deprotonation sites, the imino proton (N_1-H, pK_a=3.9) and the amino proton (N_2-H, pK_a=4.7) [1, 2, 8, 9, 12,

†Part of the special issue for "the Chinese Chemical Society's 15th National Chemical Dynamics Symposium".
*Authors to whom correspondence should be addressed. E-mail: songdi@iccas.ac.cn, hongmei@bnu.edu.cn

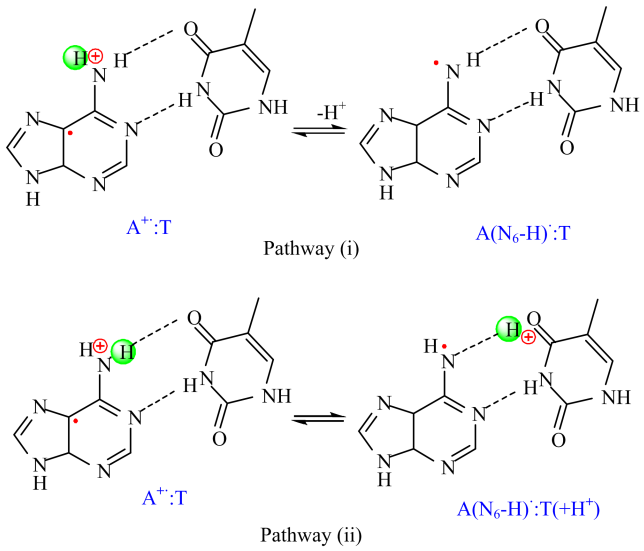

Scheme 1 Two possible deprotonation pathways of A^+ in duplex DNA.

13]. Pulse radiolysis and ESR experiments have shown that $G^{+\cdot}$ preferentially deprotonates N_1-H to generate $G(N_1\text{-H})^{\cdot}$ with the rate constant of 1.8×10^7 s^{-1} [10, 16]. Kobayashi *et al.* measured deprotonation rate constants of $(3.3-3.6)\times10^6$ s^{-1} in different duplex DNA, and suggested that the whole deprotonation process can be interpreted by the following steps: proton transfer from the base-pair cation radical $G^{+\cdot}$:C first gives deprotonated G radical and the cytosine base pair ($G(\text{-H})^{\cdot}$:$C(+H^+)$) and then the proton of $C(+H^+)$ is expected to be finally picked up by a water molecule [10]. Recently, our group used nanosecond laser flash photolysis to investigate the deprotonation of 1-methylguanine (mG), of which N_1-H is substituted by methyl group, and thus obtained the rate constant and activation energy of deprotonation from N_2-H [12]. Further, our group also examined the unique deprotonation behaviors of G-quadruplexes, revealing the unusual deprotonation site of amino proton N_2-H and much slower rate constants of $(1.8-2.1)\times10^5$ s^{-1} in G-quadruplexes that are different from duplex DNA [13].

Adenine (A) owns a low oxidation potential ($E^{\ominus}$=1.42 V *vs.* NHE) comparable to G, thus can readily undergo the oxidation to $A^{+\cdot}$ [1, 11, 18]. However, different from intensive reports for $G^{+\cdot}$, studies on deprotonation of $A^{+\cdot}$ are limited. According to the structure of $A^{+\cdot}$, there is merely one active proton N_6-H that can be released to generate $A(N_6\text{-H})^{\cdot}$ (FIG. 1) [1, 11]. Pulse radiolysis experiments and low temperature ESR experiments had verified the deprotonation site [11, 19]. The pulse radiolysis experiments also showed that the deprotonation rate constant measured in duplex DNA (2.0×10^7 s^{-1}) was similar to that in free A base, which seemed to suggest that the N_6-H proton of $A^{+\cdot}$ in duplex DNA is directly released to the solvent, as in the case of free A (Scheme 1, pathway (i)) [11]. An alternative deprotonation pathway (Scheme 1, pathway (ii)), that is, the proton transfer from N_6-H of A to the O atom of Thymine (T) within the $A^{+\cdot}$:T base pair, was ruled out by Steenken because the pK_a values of $A^{+\cdot}$ (pK_a=4.0) [11, 18, 20] and $T(+H^+)$ (pK_a=−5) make this pathway infeasible [1, 14]. However, a gas phase B3LYP/6-31G** calculation of relative stabilities of $A^{+\cdot}$:T (reactant) and $A(N_6\text{-H})^{\cdot}$:$T(+H^+)$ (product) showed that the pathway (ii) is endothermic by 5.0 kJ/mol and there is only a small barrier of 6.7 kJ/mol [21]. The gas phase calculation results suggested that pathway (ii) could possibly occur, which is in contradiction with the experimental results [14, 21]. It follows that further studies are required to clarify the $A^{+\cdot}$ deprotonation process.

Herein, we performed joint experimental and theoretical investigations on the deprotonation reaction of $A^{+\cdot}$. The one-electron oxidation of A to $A^{+\cdot}$ and its subsequent deprotonation product, $A(N_6\text{-H})^{\cdot}$, were detected in the time-resolved UV-Vis absorption spectra. By monitoring the formation kinetics of $A(N_6\text{-H})^{\cdot}$, the deprotonation rate constants were measured at different temperatures varying from 280 K to 300 K. Based on Arrhenius equation, the activation energy barrier for the N_6-H deprotonation is thus determined to be 17.1 kJ/mol. Theoretically, we calculated potential energy surface (PES) of the deprotonation process of $A^{+\cdot}$ under solvation models including both explicit waters and the polarized continuum model (PCM). The energy barrier obtained from the PES (18.2 kJ/mol) is coincident with our experimental value, implying the rationality of the current theoretical treatments. Based on the theoretical treatments, we also performed calculations for the pathways (i) and (ii) of $A^{+\cdot}$:T in duplex DNA, and discussed the $A^{+\cdot}$ deprotonation pathway in duplex DNA from dynamics considerations. These experimental and theoretical results can provide valuable dynamics and mechanistic insights for oxidative DNA damage and potential application in DNA-based electrochemical devices.

II. MATERIALS AND METHODS

A. Materials

2′-Deoxyadenine (A, Alfa Aesar), sodium persulfate ($Na_2S_2O_8$, Sigma-Aldrich), and sodium phosphate buffer (50 mmol/L, Beijing Solarbio Science & Technology) were used as purchased. Ultrapure water obtained by Millipore filtration was used as solvent. The samples of A and $Na_2S_2O_8$ were dissolved in 3 mL of sodium phosphate buffer in H_2O. Note that each kinetic measurement was performed with new sample.

B. Laser flash photolysis

Nanosecond time-resolved UV-Vis transient absorption spectra were measured using a flash photoly-

DOI:10.1063/1674-0068/30/cjcp1710198

sis setup Edinburgh LP920 spectrometer (Edinburgh Instruments Ltd.) combined with a Nd:YAG laser (Spectra-Physics Lab 170, Newport Corp.). Each measurement was performed in a 1 cm path length quartz cuvette that was put in the Oxford Instruments OptistatDN Cryostat and cooled to a certain temperature. The sample was excited by using a 355 nm laser pulse (1 Hz, 10 mJ/pulse, fwhm≈7 ns). The analyzing light was from a 450 W pulsed xenon lamp. A monochromator equipped with a photomultiplier for collecting the spectral range from 300 nm to 700 nm was used to analyze transient absorption spectra. The signals from the photomultiplier were displayed and recorded as a function of time on a 100 MHz (1.25 Gs/s sampling rate) oscilloscope (TDS 3012C, Tektronix), and the data were transferred to a PC. Data were analyzed with online software of the LP920 spectrophotometer and instrument response function of Gaussian type was considered. The fitting quality was judged by weighted residuals and reduced χ^2 value.

C. Computational methods

The geometries of the reactants, products, and transition states were optimized using B3LYP in connection with the 6-31++G** basis set in PCM model, which have been shown to be a sufficient and affordable computational method for studying DNA base [16, 22]. The harmonic frequency analysis was performed to identify the stationary points as either local minima (reactants and products) or first order saddle points (transition states) and to extract zero-point vibrational energy (ZPE) corrections. Connections of the transition states between two local minima were confirmed by intrinsic reaction coordinate (IRC) calculations at the same level. The charges from natural bond orbital (NBO) results and the spin densities, were evaluated at the same level to characterize the proton transfer of the PES. All the calculations were carried out using the Gaussian 09 program package [23].

III. RESULTS AND DISCUSSION

A. Transient absorption spectra of $A^{+\cdot}$ and its deprotonation product $A(N_6\text{-}H)^{\cdot}$

Sulfate radicals, $SO_4^{-\cdot}$, were produced by the 355 nm laser photo-dissociation of peroxodisulfate anions ($S_2O_8^{2-\cdot}$) (Eq.(1)) [12, 13, 17]. The instantaneously generated $SO_4^{-\cdot}$ further oxidizes A to $A^{+\cdot}$ and $A^{+\cdot}$ subsequently deprotonates to neural radical $A(N_6\text{-}H)^{\cdot}$ (Eq.(2) and Eq.(3)) [11].

$$S_2O_8^{2-} \xrightarrow{h\nu} 2\ SO_4^{-\cdot} \qquad (1)$$

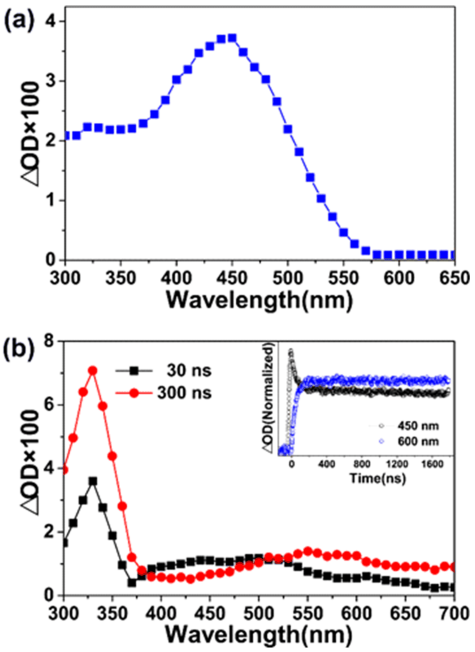

FIG. 2 (a) Transient UV-Vis spectrum at 30 ns for buffer solution (pH=7.5) of $Na_2S_2O_8$ (500 mmol/L) upon 355 nm laser excitation. (b) Transient UV-Vis spectra monitored at 30 ns (black square) and 300 ns (red circle) for buffer solution (pH=7.5) of A (6 mmol/L)+$Na_2S_2O_8$ (500 mmol/L) upon 355 nm laser excitation. Inset: kinetics traces for $A^{+\cdot}$ decay at 450 nm and $A(N_6\text{-}H)^{\cdot}$ growth at 600 nm.

$$SO_4^{-\cdot} + A \rightarrow SO_4^{2-} + A^{+\cdot} \qquad (2)$$

$$A^{+\cdot} \rightarrow A(N_6\text{-}H)^{\cdot} + H^+ \qquad (3)$$

The transient absorption of sulfate radical $SO_4^{-\cdot}$ is featured with the resolved band at 450 nm and a shoulder at 330 nm (FIG. 2(a)), which agrees with previous spectra [4, 10, 12, 13]. The rapid photodissociation of $S_2O_8^{2-}$ results in the generation of $SO_4^{-\cdot}$ within the ∼14 ns laser pulse duration. As a result, the formation dynamics of $SO_4^{-\cdot}$ does not interfere with the detection for the subsequent oxidation reaction of $SO_4^{-\cdot}$+A (Eq.(2)). The concentration of $SO_4^{-\cdot}$ can be estimated by the absorbance at 450 nm using an extinction coefficient of 1600 $(mol/L)^{-1}cm^{-1}$ [4, 10, 12, 13], which is ∼25 μmol/L and much smaller than the concentration of A (6 mmol/L). The large excess concentration of A ensures the oxidation reaction of A by SO_4^- is a pseudo-first order reaction, and excludes the possibilities of sequential oxidation events of A.

For the oxidation of A+$SO_4^{-\cdot}$ at room temperature (FIG. 2(b)), one strong peak at 330 nm and a weak and flat absorption from 380 nm to 700 nm (absorption maxima around 500 nm), are exhibited in the early time (30 ns) transient spectrum, which are essentially similar to those reported before and can be identified as those of $A^{+\cdot}$ [11]. It is noticeable that the 355 nm photolysis of A alone does not generate any signal.

As the reaction proceeds with time, the absorbance of

DOI:10.1063/1674-0068/30/cjcp1710198

the peak at 330 nm and the broad band from 550 nm to 700 nm increases, while the absorbance around 450 nm decays in the 300 ns spectrum (FIG. 2(b)). This transient spectrum is ascribed to the A(N_6-H)$^{\cdot}$ radical, which is featured with a strong peak at 330 nm and a weak absorption from 450 nm to 700 nm, with absorption maximum around 550 nm [11]. Furthermore, the inset of FIG. 2(b) also shows that the decay at 450 nm corresponds to the absorbance increase at 600 nm, meaning that the two absorbance changes should originate from the same reaction process, that is, the deprotonation of $A^{+\cdot}$ to A(N_6-H)$^{\cdot}$.

B. The measurement of deprotonation rate constant of $A^{+\cdot}$

The one-electron oxidation to form $A^{+\cdot}$ is accompanied by fast deprotonation to A(N_6-H)$^{\cdot}$. To discern the deprotonation of $A^{+\cdot}$, the A concentration dependence of the reaction kinetics was studied. As shown FIG. 2(b), the absorption spectrum of A(N_6-H)$^{\cdot}$ exhibits a stronger absorption from 550 nm to 700 nm than that of $A^{+\cdot}$, the absorbance changes at 600 nm were thus measured. FIG. 3(a) shows the dependence of the apparent rate constants on the concentration of A. The plot of rate constant versus the concentration of A exhibits a linear relationship below 5 mmol/L, indicating that the rate-determining step is the bimolecular reaction of A with $SO_4^{-\cdot}$. From the slope, the second-order rate constant of the reaction with $SO_4^{-\cdot}$ is obtained to be $(4.0\pm0.2)\times10^9$ $(mol/L)^{-1}s^{-1}$. The rate constant reached a plateau above 5 mmol/L, and thus the saturated rate constant, $(2.0\pm0.1)\times10^7$ s^{-1}, is ascribed to the first-order deprotonation process of $A^{+\cdot}$ which should be independent of the A concentration. The deprotonation rate constant measured here in laser flash photolysis agrees well with that measured by pulse radiolysis (2.0×10^7 s^{-1}) [11]. By performing experiments at high A concentration, reactions (Eq.(2) and Eq.(3)) can be kinetically resolved.

C. The measurement of the activation energy of $A^{+\cdot}$ deprotonation

The better assessment of the deprotonation processes of $A^{+\cdot}$ to A(N_6-H)$^{\cdot}$ requires the knowledge of the dynamics data, not only the rate constant but also the activation energy barrier. To obtain the activation energy of the $A^{+\cdot}$ deprotonation, the deprotonation rate constant as a function of temperature in the range of 280−300 K was measured (FIG. 3(b)). The concentration of A of 6 mmol/L was employed at each temperature to ensure that deprotonation is the rate-determining step. As shown in FIG. 3(b), the deprotonation rate constants decrease with the decreasing temperature, and the rate constants exhibit an Arrhenius behavior.

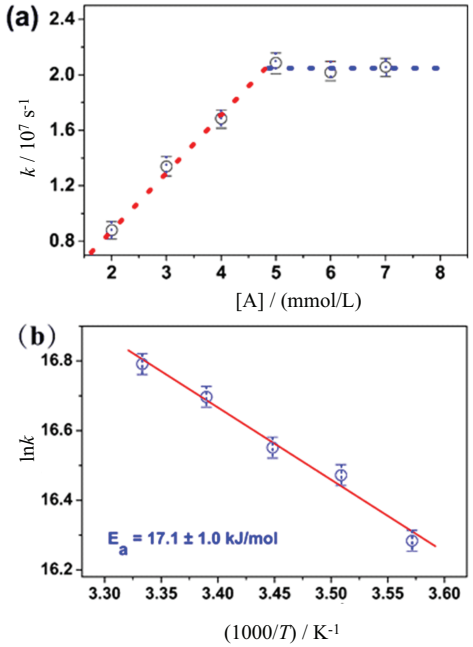

FIG. 3 (a) A concentration dependence of A(N_6-H)$^{\cdot}$ formation rate constant obtained from the absorbance increasing changes at 600 nm. (b) Arrhenius plot for the temperature dependence (280, 285, 290, 295, and 300 K) of the deprotonation rate constants obtained from the absorbance increasing changes at 600 nm, with the activation energy indicated. Solid red line is the fit.

$$\ln k = \ln A - \frac{E_a}{RT} \tag{4}$$

The Arrhenius plot yields an E_a value equal to (17.1±1.0) kJ/mol (Eq.(4), FIG. 3(b)), which corresponds to the activation energy barrier of the deprotonation processes of $A^{+\cdot}$ to A(N_6-H)$^{\cdot}$. This small energy barrier, (17.1±1.0) kJ/mol, can also interpret the rapid deprotonation process of $A^{+\cdot}$ to A(N_6-H)$^{\cdot}$.

In addition, we also tried to measure the activation energy barrier of the deprotonation of $A^{+\cdot}$ in duplex DNA. However, the present experimental conditions cannot fulfill the requirement of high concentration of duplex DNA (above 5 mmol/L), and the activation energy of $A^{+\cdot}$ in duplex DNA thus was not obtained.

D. Theoretical study of deprotonation process of $A^{+\cdot}$ in free base

Here, the experimentally determined energy barrier for the $A^{+\cdot}$ deprotonation (17.1±1.0 kJ/mol) is quite different from the value (6.7 kJ/mol) predicted by gas phase theoretical calculations [21]. The gas phase calculations obviously ignored the fact that the reaction takes place in aqueous solution. So the solvent effect has to be considered carefully to model the reaction process

DOI:10.1063/1674-0068/30/cjcp1710198

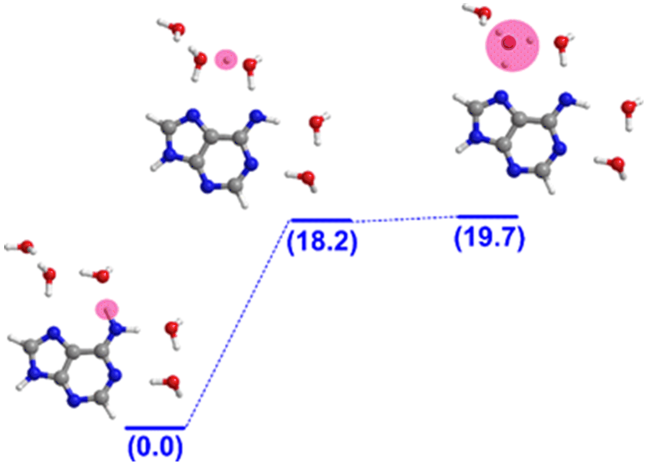

FIG. 4 Potential energy profile for the deprotonation pathway of $A^{+\cdot}$ under the solvation model including five explicit waters and PCM, kJ/mol. Optimized geometries are also plotted. Carbon, oxygen, nitrogen, and hydrogen atoms are denoted with gray, red, blue, and white balls, respectively. The pink circle highlights the migrated proton.

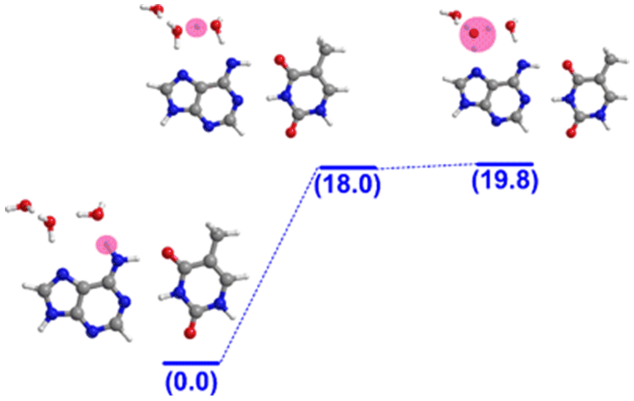

FIG. 5 Potential energy profile for the deprotonation pathway (i) of $A^{+\cdot}$:T under the solvation model including 3 explicit waters and PCM, kJ/mol. Optimized geometries are also plotted. Carbon, oxygen, nitrogen, and hydrogen atoms are denoted with gray, red, blue, and white balls, respectively. The pink circle highlights the migrated proton.

[22, 24, 25]. Therefore, we mimicked the solvation of $A^{+\cdot}$ by using a combined explicit water and bulk water approach which has been successfully testified in the $G^{+\cdot}$ system [22, 24]. The five explicit water molecules are used to reflect the specific short-range interactions around the deprotonation site while the PCM is used to treat the remaining bulk water.

Under this solvation model, we first calculated the PES for the deprotonation process of $A^{+\cdot}$ in free A base. The geometries of $A^{+\cdot}$ (reactant), $A(N_6\text{-}H)^{\cdot}$(product) and the transition state (TS) $[A^{\cdot}\cdots H^{+}]$ for the deprotonation process of $A^{+\cdot}$ in the presence of 5 explicit water molecules were fully optimized using density functional theory (DFT) B3LYP and the 6-31++G** basis set. Frequency analysis was also performed, at the same level of theory and basis set, to ensure the existence of reactant and product as local energy minimum, and for the TS, a negative frequency was found.

FIG. 4 displays the PES for the deprotonation of $A^{+\cdot}$ to $A(N_6\text{-}H)^{\cdot}$ in free base. Initially, the reactant $A^{+\cdot}$ and the five water molecules form a complex $A^{+\cdot}\cdots 5H_2O$. Accompanying the cleavage of N_6-H bond, a transition state (TS) with an energy barrier of 18.2 kJ/mol was located. NBO results show that the proton H^+ is finally stabilized at the H_2O near N_7 site of A, leading to the formation of the deprotonation product $A(N_6\text{-}H)^{\cdot}$ (FIG. 4). The PES clearly describes how the proton H^+ is released from $A^{+\cdot}$ to the first hydration shell as represented by the explicit water, revealing the deprotonation mechanism of $A^{+\cdot}$. As for the proton further migrating to the outer hydration shell, it has been proved to be very efficient [26, 27]. Therefore, the transport of H^+ to the first hydration shell is supposed to be the rate-determining step for $A^{+\cdot}$ deprotonation. The calculated reaction energy barrier of 18.2 kJ/mol thus can be approximately regarded as the activation energy for the overall deprotonation process of $A^{+\cdot}$, which is in good agreement with the experimental value of 17.1 kJ/mol.

It should be noted that we also tested the effect of the number and the position of the explicit waters. First, increasing more waters far away from the $A^{+\cdot}$ deprotonation site does not change the energy barrier, indicating the influence of the water molecules far from the deprotonation site is not significant for deprotonation process of $A^{+\cdot}$. Second, with the use of less explicit waters, the energy barrier becomes much lower than the experimental value. For example, the energy barrier under the three explicit water model is only 10.9 kJ/mol. Hence, it can be deduced that the use of five waters is suitable for elaborating deprotonation mechanism of $A^{+\cdot}$. The agreement with the experiment also demonstrates the rationality of the current theoretical treatments.

E. Theoretical study of deprotonation process of $A^{+\cdot}$:T in duplex DNA

Based on the theoretical treatments of $A^{+\cdot}$ deprotonation, we also performed DFT calculations for the two possible deprotonation pathways (Scheme 1) of $A^{+\cdot}$:T in duplex DNA. The AT base pair is used here as a simplified duplex unit to save the computational costs. In this base pair, N_1 and N_2 of A separately form two hydrogen bonds with H_3 and O_4 of T, three explicit waters are thus used in the following calculations.

The PES for the deprotonation pathway (i) (Scheme 1) that involves the direct release of N_6-H proton of $A^{+\cdot}$ to the solvent is shown in FIG. 5. The reactant $A{:}T^{+\cdot}$ and the three explicit water molecules form an expected complex $A^{+\cdot}{:}T\cdots 3H_2O$. Starting from the

DOI:10.1063/1674-0068/30/cjcp1710198

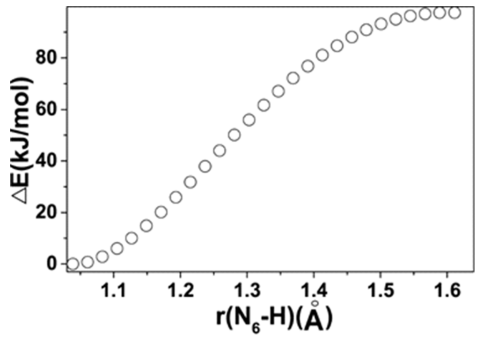

FIG. 6 Energy variation of $A^{+\cdot}$:T with the increasing of N_6-H bond length under the solvation model including 3 explicit waters and PCM, kJ/mol.

initial structure, the deprotonation of $A^{+\cdot}$:T to A(N_6-H)$^{\cdot}$:T requires a reaction energy barrier of 18.0 kJ/mol, which agrees with the activation energy for the deprotonation of $A^{+\cdot}$ in free base (experimental value 17.1 kJ/mol, theoretical value 18.2 kJ/mol). Hence, by incorporating the solvent effect based on explicit water and PCM model, our calculations can well interpret the experimental results [11] that similar deprotonation rate constants of $A^{+\cdot}$ were observed in the free A base and in duplex DNA, suggesting that the N_6-H proton of $A^{+\cdot}$ in duplex DNA should be directly released to the solvent, as in the case of free A.

For the deprotonation pathway (ii) (Scheme 1) that occurs through the proton transfer within the AT base pair, the previous calculation in the gas phase suggested it could possibly occur [21]. However, the calculation ignored the solvent effect, which might not accurately describe the deprotonation of $A^{+\cdot}$ in duplex DNA [14]. In this work, we attempted to locate the structures of the product A(N_6-H)$^{\cdot}$:T(+H^+) and the transition state [$A^{\cdot}\cdots H^+\cdots$ T] with inclusion of three or more explicit waters based on the optimized structures in Ref.[21]. However, it was found that the product and the transition state could not be located and always converged to the structure of reactant $A^{+\cdot}$:T, no matter with or without PCM model. In this case, we further scanned the proton transfer coordinate N_6-H bond length and obtained corresponding energy variation (FIG. 6). It is found that the energy increases with the increasing of N_6-H bond length monotonically. These results indicate that the N_6-H proton transfer along the hydrogen bond within AT base pair (pathway (ii)) hardly occurs, supporting the postulation [1, 14] that the pK_a values of $A^{+\cdot}$ (pK_a=4.0) and T(+H^+) (pK_a=−5) make the proton transfer within the AT base pair infeasible. Considering quite low energy barrier (18.0 kJ/mol) of the pathway (i), it can thus be deduced that the deprotonation process of $A^{+\cdot}$:T in duplex DNA follows the pathway (i): the N_6-H proton of $A^{+\cdot}$ in duplex DNA is directly released to the solvent, as in the case of free A (Scheme 1, pathway (i)).

IV. CONCLUSION

In this work, we have experimentally and theoretically investigated the deprotonation behavior of $A^{+\cdot}$. The highly potent radical $SO_4^{-\cdot}$ was used to oxidize A, generating $A^{+\cdot}$. The time-resolved UV-Vis absorption spectra showed the formation of deprotonation product of A(N_6-H)$^{\cdot}$. The rate constants of A+$SO_4^{-\cdot}$ oxidation and $A^{+\cdot}$ deprotonation were measured to be 4.0×10^9 (mol/L)$^{-1}$ s^{-1} and 2.0×10^7 s^{-1} at room temperature, respectively. Further, the formation kinetics of A(N_6-H)$^{\cdot}$ at various temperatures were measured, from which the activation energy barrier for $A^{+\cdot}$ deprotonation was determined to be 17.1 kJ/mol. To gain mechanistic insights, we performed DFT calculations for describing the $A^{+\cdot}$ deprotonation under the solvation models including both explicit waters and PCM. The calculated PES reveals an energy barrier (18.2 kJ/mol) that matches with our experimental value, suggesting the reliability of the current theoretical treatment for $A^{+\cdot}$ deprotonation. Based on this strategy, we also calculated and assessed the $A^{+\cdot}$ deprotonation pathways in duplex DNA. For the deprotonation pathway (i) of $A^{+\cdot}$:T in duplex DNA (Scheme 1, pathway (i)), the calculated energy barrier (17.8 kJ/mol) agrees with both experimental and calculated values of $A^{+\cdot}$ in free base, suggesting that similar deprotonation pathway of $A^{+\cdot}$ occurs in duplex DNA to that in free base, undergoing direct release of the N_6-H to aqueous solvent. Whereas, the deprotonation pathway (ii) of $A^{+\cdot}$:T involving the proton transfer along the hydrogen bond within AT base pair was found to be energetically infeasible, confronting an energy increase monotonically with the increase of the N_6-H bond distance (Scheme 1, pathway (ii)). These results have provided the kinetics energy barrier data and clarified the deprotonation behavior of $A^{+\cdot}$ in both free A base and in AT base pair of duplex DNA, which should be of value for understanding the oxidative DNA damage and guiding related applications in adenine DNA-based electronics devices.

V. ACKNOWLEDGMENTS

This work was supported by the National Natural Science Foundation of China (No.21425313, No.21333012, No.21373233, and No.91441108) and the Chinese Academy of Sciences (No.XDB12020200).

[1] S. Steenken, Chem. Rev. **89**, 503 (1989).
[2] L. P. Candeias and S. Steenken, J. Am. Chem. Soc. **114**, 699 (1992).
[3] M. K. Kuimova, A. J. Cowan, P. Matousek, A. W. Parker, X. Z. Sun, M. Towrie, and M. W. George, Proc. Natl. Acad. Sci. USA **103**, 2150 (2006).

DOI:10.1063/1674-0068/30/cjcp1710198

[4] Y. Rokhlenko, N. E. Geacintov, and V. Shafirovich, J. Am. Chem. Soc. **134**, 4955 (2012).
[5] Q. Du, H. M. Zhao, and H. M. Su, Chin. J. Chem. Phys. **26**, 661 (2013).
[6] T. Lindahl, Nature **362**, 709 (1993).
[7] A. Lapi, G. Pratviel, and B. Meunier, Met. Based Drugs. **8**, 47 (2001).
[8] L. Candeias and S. Steenken, J. Am. Chem. Soc. **111**, 1094 (1989).
[9] S. Steenken, Free Radical Res. Commun. **16**, 349 (1992).
[10] K. Kobayashi and S. Tagawa, J. Am. Chem. Soc. **125**, 10213 (2003).
[11] K. Kobayashi, J. Phys. Chem. B. **114**, 5600 (2010).
[12] L. D. Wu, J. L. Jie, K. H. Liu, and H. M. Su, Acta Chim. Sin. **72**, 1182 (2014).
[13] L. D. Wu, K. H. Liu, J. L. Jie, D. Song, and H. M. Su, J. Am. Chem. Soc. **137**, 259 (2014).
[14] A. Kumar and M. D. Sevilla, Chem. Rev. **110**, 7002 (2010).
[15] G. V. Buxton, C. L. Greenstock, W. P. Helman, and A. B. Ross, J. Phys. Chem. Ref. Data **17**, 513 (1988).
[16] A. Adhikary, A. Kumar, D. Becker, and M. D. Sevilla, J. Phys. Chem. B **110**, 24171 (2006).
[17] J. L. Jie, K. H. Liu, L. D. Wu, H. M. Zhao, D. Song, and H. M. Su, Sci. Adv. **3**, e1700171 (2017).
[18] R. Scheek, S. Stob, T. Schleich, N. Alma, C. Hilbers, and R. Kaptein, J. Am. Chem. Soc. **103**, 5930 (1981).
[19] A. Adhikary, A. Kumar, D. Khanduri, and M. D. Sevilla, J. Am. Chem. Soc. **130**, 10282 (2008).
[20] D. M. Close, J. Phys. Chem. A **117**, 473 (2013).
[21] J. Bertran, A. Oliva, L. Rodríguez-Santiago, and M. Sodupe, J. Am. Chem. Soc. **120**, 8159 (1998).
[22] A. Kumar and M. D. Sevilla, J. Phys. Chem. B **113**, 11359 (2009).
[23] M. J. Frisch, G. W. Trucks, H. B. Schlegel, G. E. Scuseria, M. A. Robb, J. R. Cheeseman, G. Scalmani, B. M. V. Barone, H. N. G. A. Petersson, M. Caricato, X. Li, H. P. Hratchian, J. B. A. F. Izmaylov, G. Zheng, J. L. Sonnenberg, M. Hada, K. T. M. Ehara, R. Fukuda, J. Hasegawa, M. Ishida, T. Nakajima, O. K. Y. Honda, H. Nakai, T. Vreven, J. A. Montgomery Jr., F. O. J. E. Peralta, M. Bearpark, J. J. Heyd, E. Brothers, V. N. S. K. N. Kudin, T. Keith, R. Kobayashi, J. Normand, , A. R. K. Raghavachari, J. C. Burant, S. S. Iyengar, J. Tomasi, N. R. M. Cossi, J. M. Millam, M. Klene, J. E. Knox, J. B. Cross, C. A. V. Bakken, J. Jaramillo, R. Gomperts, R. E. Stratmann, , A. J. A. O. Yazyev, R. Cammi, C. Pomelli, J. W. Ochterski, K. M. R. L. Martin, V. G. Zakrzewski, G. A. Voth, J. J. D. P. Salvador, S. Dapprich, A. D. Daniels, , J. B. F. O. Farkas, J. V. Ortiz, J. Cioslowski, and D. J. Fox., *Gaussian 09, Revision E.01*. Pittsburgh, PA: Gaussian, Inc., (2013).
[24] J. P. Cerón-Carrasco, A. Requena, E. A. Perpète, C. Michaux, and D. Jacquemin, J. Phys. Chem. B **114**, 13439 (2010).
[25] B. Thapa and H. B. Schlegel, J. Phys. Chem. A **119**, 5134 (2015).
[26] D. Song, H. M. Su, F. A. Kong, and S. H. Lin, J. Phys. Chem. A **114**, 10217 (2010).
[27] D. Song, H. M. Su, F. A. Kong, and S. H. Lin, J. Chem. Phys. **138**, 104301 (2013).

DOI:10.1063/1674-0068/30/cjcp1710198